

# Nanoscale-crystallite nucleation and growth in amorphous solids

A. B. Pevtsov, V. Yu. Davydov, and N. A. Feoktistov  
*A. F. Ioffe Physico-Technical Institute, 194021, St. Petersburg, Russia*

V. G. Karpov  
*State Technical University, 195251 St. Petersburg, Russia*  
(Received 28 November 1994)

A model is proposed to describe the crystallization in disordered solids. The model is based on accounting for small statistical fluctuations in structural parameters (valence angles, bond lengths, etc.), which are shown to affect the crystallization kinetics dramatically. As opposed to the standard approach that neglects any effects due to disorder, the model reveals clearly divided stages of nucleation, growth, and ripening in the crystallization of one-component disordered solids. We show that at the nucleation stage the crystallization is nonlinear in time and is bounded by a certain small volume fraction ( $\approx 0.1$ ). At the growth stage the radius of the crystallites depends on time logarithmically and approximately double its initial value until the ripening stage comes. The results of Raman light-scattering experiments designed to test various predictions of the model are presented for  $\alpha$ -Si:H subjected to crystallization. Good agreement is obtained.

## I. INTRODUCTION

Amorphous solids are normally far from thermal equilibrium. They therefore try to adjust their frozen-in structures towards their equilibrium crystalline forms. These relaxation rates are typically very slow as compared to the experimental times. Adding energy to the system accelerates the relaxation. In particular, heating an amorphous solid well below its melting temperature in many cases leads to its crystallization.

Although the microscopic reasons behind this type of transformation are at present not well understood, a phenomenological approach has been widely employed<sup>1-3</sup> to describe the transformations along the standard lines of the first-order phase transition theory. In the same spirit as the latter theory the approach is based on considering the conception and posterior growth of crystalline embryos in an amorphous matrix. Surprisingly, no attention has been paid to that approach to the static disorder which is intrinsic to amorphous solids.

Recently attention has focused on disorder-induced effects in the first-order phase transformations in solids: in Refs. 4 and 5 a particular case of diffusive decomposition in disordered solids has been considered. It was argued that the static disorder, frozen-in or caused by impurities, influences both the nucleation and ripening stages of diffusive decomposition dramatically. It is then natural to extend this concept to the case of crystallization in amorphous solids.

In this paper the emphasis will be placed on a description of the effects due to static disorder in amorphous phase. While the short-range-order topology in the ensemble of structural units ("elemental cells") of an amorphous solid is normally conserved,<sup>6</sup> their microscopic parameters (valence angles, bond lengths, etc.) fluctuate, leading to corresponding fluctuations in atomic energies

and thus local fluctuations in the free energy difference between the two phases and in the interfacial energy. By static fluctuations we mean those of lifetimes much longer than both the times of nucleation and growth processes. That is why these processes are expected to proceed differently in different local regions of an amorphous solid.

The idea is that there are some local favorable inhomogeneities in randomly disordered media, which effectively decrease thermodynamic barriers to nucleation and, thus, increase the nucleation rate exponentially. On the other hand, there should be some unfavorable local configurations of the disorder, which do not contribute much to the nucleation rate, while they slow down the growth velocity. We show that because of the disorder, the crystallite radii depend on time logarithmically and, thus, the growth rate is considerably smaller than the nucleation rate. Also, we show that available for nucleation is a certain small relative volume  $v_c \ll 1$ , beyond which the nucleation slows down abruptly. As a result crystallites of almost the same radii appear at the nucleation stage and then grow with a time logarithmically. The growth stage ends when the crystallites possessing different orientations of their crystallographic axes come in touch with each other. From that moment on the ripening stage develops at which the crystallization is slowed down still more since it is then necessary to reorient some crystallites in order for the ripening to be possible.

The paper is organized as follows. In Sec. II we consider both the standard approach and an original model to describe crystallization in amorphous solids. The model yields predictions for both the nucleation, growth, and ripening stages of crystallization and substantiates the possibility to discriminate between these stages as such. In Sec. III we present experimental results on the crystallization kinetics in  $\alpha$ -Si:H. Raman-light-scattering experiments are described and the recipe is given to trace the crystallization kinetics by means of

those experiments. Also, in Sec. III we compare the experimental results with the predictions of our model; we find that all observed effects can be understood in the framework of the model proposed. In Sec. IV some concluding remarks are given.

## II. CRYSTALLIZATION IN DISORDERED SOLIDS

### A. Standard approach

Let us first review the basic equations of the standard theory of crystallization in solids.<sup>1-3</sup> A crystalline phase is supposed to appear in the form of critical embryos which then grow by simple accretion atoms from the outer amorphous matrix. Supposing the embryo has a spherical shape, its formation changes the free energy by

$$F_c(R) = -\frac{4\pi R^3}{3}\mu + 4\pi R^2\sigma, \quad (1)$$

where  $R$  is the embryo radius,  $\mu (> 0)$  is the free energy difference between the two phases per unit volume, and  $\sigma$  is the interfacial energy per unit area. The function  $F_c(R)$  reaches its maximum

$$W = \max_R F_c(R) = \frac{16\pi\sigma^3}{3\mu^2} \quad (2)$$

at the critical radius  $R_c = 2\sigma/\mu$ . An embryo grows at  $R > R_c$ , while it disappears at  $R < R_c$ . The number of stable embryos per unit time per unit volume is given by the nucleation rate

$$I = I'_0 \exp\left(-\frac{V}{kT} - \frac{W}{kT}\right) \equiv I_0 \exp\left(-\frac{W}{kT}\right), \quad (3)$$

where  $V$  is the barrier to overcome in order for an atomic particle to join an embryo and  $k$  is Boltzmann's constant. The preexponential factor  $I'_0$  varies from  $10^{30}$  to  $10^{35}$   $\text{s}^{-1} \text{cm}^{-3}$  depending on the particular theory in use. An estimate to serve as a rough guide is  $\nu/R_c^3$ , where  $\nu$  is the characteristic atomic frequency in a solid ( $\nu \sim 10^{13} \text{ s}^{-1}$ ). The quantities  $V$  and  $W$  are usually termed as the kinetic and thermodynamic barriers to nucleation, respectively.

A stable embryo ( $R > R_c$ ) is supposed to grow with the velocity

$$u = u_0 \exp\left(-\frac{V}{kT}\right) \left[1 - \exp\left(-\frac{\Omega}{kT}\right)\right]. \quad (4)$$

The preexponential factor  $u_0$  is typically of the order of  $10^5$   $\text{cm/s}$  (roughly estimated as  $a\nu$ , where  $a$  is the characteristic interatomic length in a solid). The multiplier in square brackets on the right-hand side in Eq. (4) reflects the possibility of a backward process in case the energy  $\Omega$  gained by a molecule in its joining an embryo is not large enough. As long as it is given by Eq. (4) the velocity does not depend on time and the nuclear radius depends on time linearly:  $R = ut$ .

Note that in spite of the fact that a particular crys-

talline particle passes through its own nucleation and growth stages, the integral process can hardly be divided into such stages in the framework of the above approach. The latter implies that while some particles have already appeared and increased their volumes by growing, the nucleation still occurs in other local regions of the system. This scenario differs considerably from that of first-order phase transitions like diffusive decomposition which are known to consist of nucleation, growth, and ripening stages. In the latter case a limitation on the nucleation time is due to the concomitant decrease in solute concentration that makes the nucleation slow down. There is no such constraint in the crystallization process unless it develops via the diffusive decomposition in a multicomponent system, in which case it is beyond the scope of our consideration.

Based on the above consideration one can define the saturation time  $t_s$  as the time needed to make the crystalline phase volume fraction dominant. This time can be roughly estimated from the condition  $R^3 n \sim 1$  with  $R = ut$  and  $n = It$ , which gives  $t_s \sim (u^3 I)^{-1/4}$ . Associated with the latter is the characteristic crystalline radius exponentially exceeding the critical radius:

$$R = ut_s \sim R_c \left[ \frac{a}{R_c} \exp\left(\frac{W}{kT}\right) \right]^{1/4} \gg R_c.$$

We note that any effects due to static disorder are ignored in the above outlined approach. Therefore, as applied to crystallization in amorphous materials, the approach implies that such effects are negligible. That the classic theory remains true in spite of a disorder was tacitly assumed in most of the preceding work dealing with crystallization in solids.

*Standard approach predictions.* We summarize this section with the predictions of the standard crystallization theory to be compared with experimental results in Sec. III below. (i) There are no clearly divided stages of nucleation and growth in the crystallization process. (ii) The embryo concentration and radii depend on temperature exponentially at any given time  $t$  well before the time of saturation  $t_s$ . (iii) Both the embryo concentration  $n(t)$  and radii  $R(t)$  are linear<sup>7</sup> in  $t$  at  $t < t_s$ . (iv) At the final stage of the process ( $t \sim t_s$ ) the average embryo radius is expected to be exponentially larger than the critical radius  $R_c$ .

### B. Nucleation rate

Although the nucleation rate in disordered media has been recently calculated in Ref. 4, nothing has been said in that paper on the temporal law  $n(t)$  in the presence of a disorder. Based on the approach in Ref. 4 this law is derived in what follows.

Associated with the change in free energy in Eq. (1) is the minimum work needed to create a spherical atomic layer of the width  $a$  and radius  $R \gg a$ ,

$$f_c(R) = a \frac{dF_c}{dR} = 6 \frac{W}{R_c^3} Ra(R_c - R). \quad (5)$$

As applied to a disordered system, a random contribution  $X_R$  must be added on the right-hand side of Eq. (5), reflecting fluctuations in microscopic structural parameters. Supposing the mean-square-root fluctuation in energy per molecule is  $v$ , the dispersion  $\Delta(R) = v^2 4\pi R^2/a^2$  must be assigned to a random quantity  $X_R$ , where  $4\pi R^2/a^2 \gg 1$  is the number of molecules in the layer. Being a sum of a large number of random contributions, the quantity  $X_R$  obeys the Gaussian statistics  $\rho(X_R) \propto \exp[-X_R^2/2\Delta(R)]$ . We therefore are in a position to estimate the probability  $P(R) \sim \exp[-f_c^2(R)/2\Delta(R)]$  of creating the layer without a loss in energy, while energy  $f_c(R) > 0$  would be expended to create such a layer in the absence of the disorder.

Since the disorder makes it possible to create atomic layers without a loss in energy, the possibility appears to decrease the barrier to nucleation. Let  $E$  be the decrease in the barrier due to static fluctuations in some favorable area of amorphous solid (see Fig. 1). Then, the nucleation rate in that area,  $I_E$ , will be exponentially increased as compared to that in Eq. (3),  $I_E = I \exp(E/kT)$ .

To estimate the probability  $P(E)$  of finding the barrier decrease larger than  $E$ , it is convenient to introduce the corresponding nuclear radius  $R_E (< R_c)$  defined by the condition that the minimum work needed to create the nucleus of radius  $R_E$  does not exceed  $W - E$ , that is,  $F_c(R_E) = W - E$  (see Fig. 1). Supposing all the subsequent layers beginning from  $R_E$  up to  $R_c$  are created without a loss in energy, the barrier to nucleation will not exceed  $W - E$  as well. It follows, then, that the probability sought is given by the product of  $N_E = (R_c - R_E)/a$  probabilities  $P(R)$  for all the above-mentioned layers:

$$P(E) = \prod_i P(R_i) \approx \prod_i \exp\left\{-\frac{[f_c(R_i)]^2}{2\Delta(R_i)}\right\} \approx \exp\left\{-\int_{R_E}^{R_c} \frac{[f_c(R)]^2}{2\Delta(R)} d\left(\frac{R}{a}\right)\right\}. \quad (6)$$

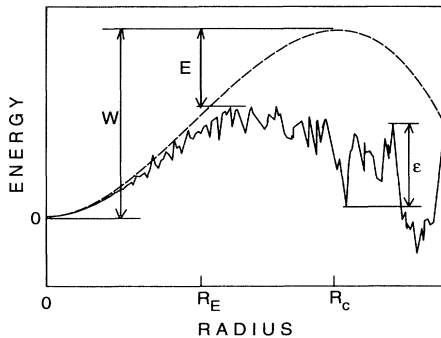


FIG. 1. Change in the free energy due to a crystalline embryo formation versus its radius  $R$  in a disordered solid (solid line) and in a homogeneous solid (dashed line).  $W$  is the classic barrier to nucleation,  $E$  is the decrease in that barrier due to fluctuations, and  $\epsilon$  is the fluctuation barrier to crystallite's growth, as is discussed in Sec. II B.

We restrict ourselves to considering the case of relatively small barrier decrease<sup>8</sup>  $E \ll W$ , which, however, allows for an exponentially large increase in the nucleation rate. The latter inequality enables one to approximate Eq. (1) by

$$F_c = W - 3\frac{W}{R_c^2}(R - R_c)^2$$

in the proximity of the barrier maximum, and, thus,  $R_c - R_E = R_c\sqrt{E/3W}$ . With that a straightforward calculation gives

$$P(E) \approx \exp\left[-\left(\frac{E}{E_0}\right)^{3/2}\right], \quad (7)$$

to within the accuracy of the preexponential factor, where

$$E_0 = (12\pi^2)^{1/3}v\left(\frac{v}{W}\right)^{1/3}\left(\frac{R_c}{a}\right)^2. \quad (8)$$

In accordance with the procedure of its derivation, Eq. (7) holds true when  $P(E) \ll 1$ , i.e.,  $E > E_0$ . It should be noted that the probability  $P(E)$  in Eq. (7) refers to the local regions which are favorable to nucleation, while there exists a comparable concentration of "difficult" regions in which the nucleation is suppressed by the disorder. For the reasons described in Sec. IID, the latter regions do not contribute to the process under consideration.

It has been tacitly assumed above that the disorder is completely uncorrelated and, thus, corresponding to different elemental cells, the local fluctuations can be regarded as mutually independent. This assumption can be equally expressed by saying that the correlation radius of a disorder is close to the characteristic interatomic distance. It is well known, however, that the static disorder in amorphous solids can possess the correlation radius  $r_c$  that considerably exceeds interatomic distances. The latter concept implies that the arrangements of structural units in an amorphous medium are not completely random but have some correlations on a scale of  $r_c$ . Estimates to serve as a rough guide can be borrowed from the neutron scattering data on a glassy state which show that  $r_c \sim 10\text{--}30 \text{ \AA}$ , varying slightly between different glasses.<sup>9-11</sup> Obviously, the above consideration holds true provided that the critical radius  $R_c$  is large in the sense  $R_c \gg r_c$  and the parameter  $a$  in Eq. (8) is replaced by  $r_c$ .

Following the approach in Ref. 4 one can optimize the nucleation rate as

$$I_{\text{opt}} = \max_E \left\{ P(E) I \exp\left(\frac{E}{kT}\right) \right\} = I \exp\left[\frac{4}{27}\left(\frac{E_0}{kT}\right)^3\right], \quad (9)$$

where  $I$  is given by Eq. (3). The optimum nucleation rate corresponds to the energy  $E_{\text{opt}} = E_0(2E_0/3kT)^2$ . Since for typical parameters in Eq. (8) the inequality obeys

$E_0 \gg kT$  (see estimates at the end of this subsection), we conclude that the nucleation rate in disordered media is exponentially larger than that of hypothetical crystal with the same average parameters. The same inequality makes the above consideration self-consistent by ensuring that  $E_{\text{opt}} \gg E_0$ .

Two comments regarding the result in Eq. (9) are in order. The first one is that fluctuations in kinetic barriers  $V$  have not been taken into account. The reasoning behind this approximation is that such fluctuations are normally characterized by the dispersion  $v^2$  related to microscopic atomic potentials, while fluctuations in thermodynamic barriers are governed by the dispersion  $\Delta(R) \sim v^2(R/a)^2 \gg v^2$  and, thus, are expected to be much more important. Another comment concerns the favorable local areas dwindling in the course of nucleation process. Supposing the nucleation is slowed down before the time  $t_{\text{opt}} \sim 1/R_c^3 I_{\text{opt}}$  of the optimum areas dwindling, the nucleation rate is described by Eq. (9). This can be the case for solid solutions where solute concentration depletion makes the nucleation slowing down in a time short enough. However, such is not necessarily the case for crystallization in amorphous solids, where the embryos of crystalline phase can appear until they fill the available volume, and, thus, not only the optimum areas have to serve as the nucleation centers.

In connection with the latter comment another reading of the result in Eq. (7) is relevant. We introduce the characteristic nucleation time

$$\tau_E = \frac{1}{I_0 R_c^3} \exp\left(\frac{W - E}{kT}\right),$$

corresponding to the local area in which the barrier to nucleation is decreased by  $E$  due to static fluctuations. For a time  $t$  the areas will be subjected to nucleation possessing the times  $\tau_E \leq t$  and corresponding barrier decreases  $E \geq E_t \equiv W - T \ln(t I_0 R_c^3)$ . The concentration of such areas  $R_c^{-3} P(E_t)$  can be regarded as that of embryos appearing throughout the time  $t$ :

$$n(t) = \frac{1}{R_c^3} \exp\left\{-\left[\frac{W - kT \ln(t I_0 R_c^3)}{E_0}\right]^{3/2}\right\}. \quad (10)$$

The interval in which the latter concentration wins over the concentration  $R_c^{-3} I_0 \exp(-W/kT)$  predicted by the classic theory is exponentially wide:

$$\frac{1}{I_0 R_c^3} \ll t \ll \frac{1}{I_0 R_c^3} \exp\left[-\left(\frac{E_0}{kT}\right)^3\right].$$

Note that given by Eq. (10) the embryo concentration is strongly nonlinear in  $t$  as opposed to that of the standard approach. Indeed, from Eq. (10) one gets

$$\frac{d(\ln v_c)}{d(\ln t)} = \left[\ln\left(\frac{1}{v_c}\right)\right]^{1/3} \frac{3kT}{2E_0}, \quad (11)$$

where  $v_c$  is the volume fraction of crystalline phase. As long as  $kT \ll E_0$ , the quantity  $v_c$  turns out to be superlinear in  $t$  at the earliest stage of nucleation ( $d \ln v_c / d \ln t > 1$ ), while it is sublinear in  $t$  if  $v_c$  is not

extremely small. Note also that the time dependence in Eq. (10) is restricted to the local regions favorable to nucleation. Therefore, it is applicable provided that the embryos take up the lesser part of the whole area. That the latter condition is met in real situations will be argued in Sec. IID.

We shall end this subsection with some remarks concerning the basic parameters appearing in the course of our consideration. As was assumed above, the short-range-order topology in the ensemble of structural units of amorphous phase is typically conserved, while their microscopic parameters (valence angles, bond length, etc.) fluctuate. These fluctuations are normally small, of the order of few percent.<sup>12</sup> Caused by these fluctuations, the above-defined mean-square-root energy fluctuation  $v$  may not be very small, since atomic potentials are extremely sensitive to random changes in microscopic structural parameters like valence angles, bond length, etc. For instance, associated with the above quantity, the relative dispersions in microscopic spring constants are estimated as  $\sim 0.1$  by means of computer modeling of different glassy structures and amorphous silicon.<sup>13,14</sup> The same order-of-magnitude estimate can be extracted from the comparison of atomic kinetics data with the theory based on accounting for statistical fluctuations in atomic potentials in glasses.<sup>15</sup> With the above in mind one can roughly estimate  $v \sim 0.1$  eV. Noting that the same statistical fluctuations are responsible for the mismatch between the crystalline and amorphous phases, the surface energy per molecule can be estimated as  $\sigma a^2 \lesssim v$ . One more energy parameter  $\mu a^3$ , the average energy difference between the two phases per molecule, can be expressed in terms of the critical nuclear radius:  $\mu a^3 = 2\sigma a^3 / R_c \sim v(a/R_c)^2$ . Since typically  $R_c \gg a$ , say,  $R_c \sim 10a$  (see Sec. III below), we get  $\mu a^3 \ll v$ . Given by Eq. (8), the energy parameter  $E_0$  can be then estimated as  $E_0 \sim v(R_c/a)^{4/3} \sim 1$  eV.

### C. Nuclear growth

We now consider the nuclear growth determining the temporal law  $R(t)$  at  $R > R_c$  in the presence of static disorder. Keeping an eye on the experiments below we will restrict ourselves to considering the average nuclear radius.

Based on the standard equation (4), two ways can be pointed out in which the disorder can affect the growth velocity. They correspond to the static fluctuations caused by the disorder in kinetic barriers  $V$  and energies  $\Omega$ , respectively. Fluctuations in kinetic barriers will be shown to make no qualitative changes in growth kinetics. To the contrary, the second cause will be shown to play a crucial role, bringing into existence a set of additional barriers to overcome in nuclear growth. These barriers turn out to increase and, thus, the growth velocity exponentially decreases with  $R$ , leading to a logarithmic dependence  $R(t)$ .

To understand the role of fluctuations in kinetic barriers we note that their probability distribution half-width must be of the order of  $v$  and that this distribution is

expected to decrease exponentially with the deviation from the average barrier  $V$ . Therefore, the number of molecules which have to surmount the diffusional barriers considerably exceeding  $V$ , will be exponentially small, and so will be the number of nuclei in which growth such molecules are involved. Caused by the disorder, the deviations  $\delta V$  from average kinetic barrier will be then typically of the order of  $v$  multiplied by some function of  $\ln N$ , where  $N$  is the number of molecules in a nucleus. Keeping an eye on the experimentally observed nuclei (see below) one can estimate  $N \sim 10^3$ – $10^4$  and thus  $\delta V \lesssim 10v$ . With that in mind the fluctuations in kinetic barriers can be accounted for by renormalizing  $V \rightarrow V + \delta V$  in Eq. (4), causing no qualitative changes in the growth kinetics.

We now consider the second of the two above-mentioned ways in which the static disorder can affect the nuclear growth. That a barrier can appear in forming an atomic layer of the radius  $R > R_c$  is not apparent immediately. Indeed, in accordance with Eq. (5) the energy decreases [ $f_c(R) < 0$ ] in forming a spherical atomic layer of the radius  $R > R_c$ , so that the average energy gain per molecule in forming the layer is

$$\Omega = \frac{f_c(R)}{4\pi(R/a)^2} = \mu a^3 \frac{R_c - R}{R}.$$

It is important that, although negative, the latter quantity is small in absolute value as compared to the dispersion:  $|\Omega| \ll v \sim \mu a^3 (R_c/a)$  (see the discussion at the end of the preceding subsection). Therefore, a considerable (although the lesser) part of molecules increases their energies by joining an embryo. That an embryo grows in spite of that increase must be attributed to the posterior capturing of the molecules which decrease their energies by joining the embryo. As long as the number of the latter molecules is larger than that of the former ones, the average nuclear energy decreases in the course of growing.

Following the above consideration we can estimate the mean-square-root fluctuation in the energy of a nucleus containing  $N$  molecules as  $\epsilon(N) = v\sqrt{N}$ . Hence, to accumulate  $N$  molecules a nucleus has typically to overcome the barrier  $\epsilon(N)$  (see Fig. 1). In other words the process of accumulating  $N \gg 1$  molecules can be described as a sort of diffusion in the energy space. The diffusion occurs via  $N$  steps, each of them decreasing or increasing the energy by  $v$  with equal probabilities. This random process is superimposed on a systematic drift caused by the energy decrease  $\Omega$  at each step.

The above reasoning implies the energy fluctuations related to different molecules to be mutually independent. In case the disorder possesses the correlation radius  $r_c > a$ , the number of independent fluctuations will be  $N(a/r_c)^3$  in place of  $N$ . Correspondingly, the barrier becomes  $\epsilon(N) = v\sqrt{N(a/r_c)^3}$ .

With the barrier  $\epsilon(N)$  taken into account Eq. (4) for the growth velocity changes to

$$u = u_0 \exp \left\{ -\frac{V}{kT} - \frac{v}{kT} \left( \frac{a}{r_c} \right)^{3/2} \sqrt{N} \right\}. \quad (12)$$

Solving the equation  $dR/dt = u$  with  $R^3 - R_c^3 = 3Nr_c^3/4\pi$  gives

$$R \approx \left\{ R_c^3 + \frac{3r_c^3}{4\pi} \left[ \frac{kT}{v} \ln \left( \frac{u_0 t}{a} \right) - \frac{V}{v} \right]^2 \right\}^{1/3}. \quad (13)$$

Hence, the crystallite radii increase with a time logarithmically.

#### D. Nucleation and growth in amorphous media

We are now in a position to compose a general scenario of crystallization in amorphous media. The basic facts are (1) the rapid increase in the nuclei concentration  $n(t)$  at the nucleation stage [in Eq. (10)] and (2) relatively weak, logarithmic nuclear radius increase  $R(t)$  [in Eq. (13)] in the course of its growing.

In the first approximation one can neglect any change in the radii throughout the nucleation time. It follows then that appearing almost simultaneously, the concentration of crystallites of almost the same radii is restricted by the free volume available for nucleation. Namely, the centers of two crystallites of the radius  $R_c$  each must be typically separated by the distance  $\Delta R$  exceeding  $4R_c$  in order that a new nucleus can appear between them. Indeed, as long as the crystallites possess different orientations of their crystallographic axes, each of the two will impose its own orientational constraint on a hypothetical new embryo that has to appear in touch with both of them in the case  $\Delta R \leq 4R$ . Since the constraints are typically mutually exclusive, each pair of nuclei separated by the distance  $\Delta R \leq 4R$  will prevent nucleation between them. Supposing a close-packed structure takes place with the distances between the spheres centers,  $4R$ , the volume fraction taken up by the spheres will be  $\approx 0.1$ . Thus, the relative volume available for nucleation can be estimated as  $\lesssim 0.1$ . Since the latter is much less than the unity, all the nuclei can be attributed to the local areas favorable for nucleation, to which the consideration in Sec. IID is applicable.

We conclude that at the first stage of crystallization a set of nuclei appears with radii close to  $R_c$  and the total relative volume  $\approx 0.1$ . At this stage the concentration of nuclei as a function of time is given by Eq. (10). Therefore, the characteristic length of this stage can be estimated as

$$\Delta t_1 \approx \frac{1}{I_0 R_c^3} \exp \left( \frac{W - E_0 (\ln v_c)^{2/3}}{kT} \right), \quad (14)$$

where  $v_c = 4\pi R_c^3 n/3 = 0.1$ .

At the second stage of crystallization new nuclei are unlikely to appear, while those appeared before grow in accordance with Eq. (13). The characteristic length of this stage over which the nuclear radius doubles can be estimated as

$$\Delta t_2 \approx \frac{a}{u_0} \exp \left[ 2.6 \frac{v}{kT} \left( \frac{R_c}{a} \right)^{3/2} + \frac{V}{kT} \right]. \quad (15)$$

After the nuclei have doubled their radii the relative volume  $0.1 \times 8 \approx 0.8$  is taken up by the crystalline phase.

On doubling their radii the nuclei come in touch with each other. From that moment and on the growth is expected to slow down even more because of the competition between the crystallites possessing different orientations of their crystallographic axes. Governed by such a competition, the growth results in both the crystallization of the remainder of amorphous phase and increase of some crystallites at the expense of the others (ripening). It is beyond the scope of this paper to describe the ripening stage of crystallization in detail. Here we restrict ourselves to saying that at the ripening stage the logarithmic time dependence  $R(t)$  is expected to survive because the system remains disordered. However, the dependence must be much slower than predicted by Eq. (13), since, caused by different random orientations of crystallites, the disorder is much stronger than that of small static fluctuations in atomic parameters.

*Our model predictions.* We summarize this section as follows. We have developed a model of crystallization in amorphous media which is based on accounting for small statistical fluctuations of microscopic atomic parameters. The predictions of the model are as follows. (i) There exist clearly divided nucleation and growth stages in the crystallization process. (ii) The concentration of nuclei increases nonlinearly with a time at the nucleation stage, being restricted by the available volume fraction  $\approx 0.1$ . The increase in nuclear radii can be neglected at the nucleation stage. (iii) Over a wide range of times at the growth stage the average nuclear radius  $R$  increases as a function of the logarithm of time multiplied by the temperature.  $R$  becomes nearly twice as large as  $R_c$  at the end of the stage. The relative volume of crystalline phase increases by a factor of 8 at this stage, while that of amorphous phase decreases by a factor of 4.5.

The above predictions differ dramatically from those of the standard approach (see Sec. II A). Such a discordance can be an important factor in choosing between the two approaches experimentally.

### III. EXPERIMENTAL RESULTS

Before dealing with any specific experiments we point out that the appearance of crystalline grains in amorphous films subjected to thermal treatments or intense laser beams has been clearly established in a number of experiments. Raman scattering experiments<sup>19–21</sup> have allowed this process to be followed as a function of annealing schedules (times, temperatures, laser intensities). Associated with such experiments is a formalism aimed at extracting information about grain sizes from the Raman scattering data.<sup>22,23</sup> Although the most recent work was devoted to porous silicon,<sup>24–26</sup> the formalism is applicable to the case of crystalline grains in amorphous materials as well.<sup>27</sup>

All the experiments to be described below refer to amorphous hydrogenated silicon, *a*-Si:H, and adequately reflect the fact that most Raman scattering experiments on crystallization performed to date have been performed

on this material. Also, it is important that the material parameters are well known for both *a*-Si:H and *c*-Si, and that the crystallization process occurs at not too high temperatures 400–500 °C. Last, *a*-Si:H remains a material of great promise in modern electronics and, thus, the study presented may offer one more controllable way of creating *a*-Si:H-based films of desired parameters.

It should be noted that the experimental results below are typical of the published data on the crystal phase in amorphous and porous silicon and on polycrystalline silicon films. Also, they have much in common with the data in crystallization in glasses. The main reason to carry out the experiments below is to obtain the whole set of data needed to verify the theory presented. The analysis of Raman spectra below also follows the standard lines except that we suggest some new interpretation of the relative Raman intensities corresponding to the crystalline and amorphous phases (Sec. III A). Although this feature is not a crucial one in deciding between the standard and our theories of crystallization, it enables one to extract more quantitative information from the measured spectra.

#### A. Analysis of Raman spectra

The analysis is based on the fact<sup>19,20,27</sup> that Raman spectra of *a*-Si:H films undergo radical changes in the course of their crystallization. Namely, associated with amorphous phase the broad low-frequency component with a maximum at about 480  $\text{cm}^{-1}$  reduces while keeping its shape nearly a constant as the temperature increases. At the same time a narrow peak nearly 520  $\text{cm}^{-1}$  arises, associated with Raman-active  $\Gamma_{25'}$  mode of crystalline silicon (*c*-Si). As opposed to the former broad component, the peak changes its intensity, position, and shape in the course of heating. The relative intensities of the two Raman components are considered as a measure of the relative amounts of amorphous and crystalline components in the material. Besides, the above-mentioned changes in narrow peak's position and shape are attributed to the corresponding changes in crystalline grains radii during the heating. Given a proper model, one can, therefore, estimate the crystalline grains radii.

The reasoning behind the latter interpretation is that a spatial confinement of optical phonons takes place because of a crystallite radius finiteness. The wave function of optical phonons is no longer a plane wave when the crystal has a finite dimension. Its localization leads to a relaxation of the conservation of crystal momentum in the creation and decay of phonons in crystallites. Allowing transitions with the wave vector  $\mathbf{q} \neq 0$  adds a contribution to the Raman spectrum at energies  $\hbar\omega$  that are determined by the dispersion relations  $\omega(\mathbf{q})$ . As long as the dispersion is negative, the additional transitions with  $\mathbf{q} \neq 0$  will lead to a broadening of the Raman line and a concomitant redshift of its mean position.<sup>27,23,28</sup>

Based on the above reasoning the crystallite Raman line shape has been shown to have a form<sup>22,23</sup>

$$I_c(\omega) = A \int_0^{q_{\max}} \frac{d^3q |C(0, \mathbf{q})|^2}{[\omega - \omega(\mathbf{q})]^2 + (\Gamma_c/2)^2}, \quad (16)$$

where  $\omega(\mathbf{q})$  and  $\Gamma_c$  are the phonon dispersion curve and natural linewidth of the bulk crystal, respectively,  $A$  is a constant, and the squared Fourier coefficient of phonon confinement function is taken as  $|C(0, \mathbf{q})|^2 = \exp(-q^2 R^2/4\pi^2)$  in the simplest approximation.

One comment is in order regarding the latter equation. It has been tacitly assumed in the course of its derivation that all the crystallites possess the same radii. Weighted with a proper size distribution function, Eq. (16) must be integrated over  $R$  to allow for the dispersion  $\delta R$  in grain radii. However, such a procedure makes almost no change in Eq. (16). The point is that the main contribution to the integral in Eq. (16) typically comes from small  $qR \ll 1$ , which statement can be verified by using various particular forms of the size distribution function. For example, using the Gaussian distribution  $\exp[-(R - \langle R \rangle)^2/\delta R^2]$  will change the exponent in Eq. (16) to  $-q^2 \langle R \rangle^2 [1 + (q\delta R)^2]^{-1}$ , where the second term in the denominator is effectively small. Besides, the conclusion that the main contribution in the integral in Eq. (16) comes from the range  $q \ll R^{-1}$  can be made on experimental grounds. Indeed, supposing the opposite is true, the integral will depend on  $R$  exponentially, contrary to the experimentally observed weak Raman line  $R$  dependence (see Refs. 27, 26, 24, and the data below). Thus, the parameter  $R$  in Eq. (16) should be regarded as the average crystallite radius, while the dispersion in crystallites radii can hardly affect that equation considerably. That is why Eq. (16) works very well as applied to the porous and microcrystalline silicon<sup>24-26</sup> in which the dispersion in crystallites radii is known to be appreciable.

As for the amorphous contribution to Raman spectra, its shape was suggested to approximate by the Lorentzian<sup>24</sup>

$$I_a(\omega) = \frac{A'\Gamma_d}{(\omega - \omega_d)^2 + \Gamma_d^2}, \quad (17)$$

where  $\omega_d$  and  $\Gamma_d$  are the material parameters and  $A'$  is a constant. Although the above approximation is rather arbitrary, we keep it in order that our consideration will be tied with the preceding results. It is believed that the observed Raman spectra can be approximated by the sum of partial contributions given by Eqs. (16) and (17). Fitting this approximation with the data enables one to extract the material parameters entering the above equations.

We must also touch upon the question about the relative intensities of the amorphous (broad) and crystalline (narrow) components of Raman spectra. The interpretation was widely employed<sup>24,27,29,25</sup> based on the belief that these intensities are simply proportional to the volume fractions of amorphous and crystalline phases. This view has its basis in the generally accepted fact that the Raman scattering intensity is proportional to the volume of a bulk sample.<sup>19</sup> In connection with that we note that the latter statement implies the sample size to be considerably larger than the light wavelength. Therefore, care should be taken to check whether such an inequality holds in the case under consideration. If we compare the characteristic crystallites sizes of the order of 100 Å with a typical wavelength  $\lambda \sim 10^4$  Å (see Refs. 27, 26, and the

data below), we see that quite opposite is true:  $\lambda \gg R$ . Hence, the above interpretation has to be reconsidered.

First of all we note that the scattering intensity is known to be proportional to the particle volume squared (not just a volume) in case the inequality  $\lambda \gg R$  obeys.<sup>16-18</sup> It would appear reasonable that different crystallites in the matrix are mutually incoherent because of the dispersion in their radii. Then, the total scattering intensity  $I_c$  due to crystallites will be proportional to  $nR^6$ . It is proportional to the crystallite volume squared and to the sample volume to the power 1. Reasoning in the same way we can divide the amorphous phase into a set of local areas of the radius  $r_c$  each, so that each area exhibits a coherent scatter, while different scatters are mutually incoherent. It is natural to identify  $r_c$  with the correlation radius in amorphous material. Then, associated with the amorphous phase, the broad component in Raman scattering can be regarded as one composed of the partial contributions corresponding to different coherent scatters. Since the concentration of such scatters is about  $(1 - 4\pi R^3 n/3)r_c^{-3}$ , the total scattering intensity  $I_a$  due to the amorphous phase is proportional to  $(1 - 4\pi R^3 n/3)r_c^3$ . As a result the ratio  $I_c/I_a$  will be

$$\frac{I_c}{I_a} = \chi \frac{4\pi n R^3/3}{1 - 4\pi R^3 n/3} \left(\frac{R}{r_c}\right)^3, \quad (18)$$

where  $\chi$  is the ratio of the squared matrix elements corresponding to the light scattering by crystalline and amorphous phase, respectively. Following the considerations in Refs. 30-32 we put  $\chi \approx 0.1$  for the case of relatively large grains with  $R \sim 50$  Å at hand. It follows from Eq. (18) that for a typical ratio  $R/r_c > 1$  the relative intensity of the crystalline component in the Raman spectra is considerably greater than the volume fraction of crystalline phase  $nR^3$ . This causes us to anticipate that Raman scattering experiments make it possible to trace the crystallization at its early, nucleation stage. Equations (16), (18), and (17) provide a basis for the interpretation of experimental results in what follows.

## B. Experimental design and results

Undoped films of hydrogenated amorphous silicon were prepared by the conventional plasma-enhanced chemical vapor deposition (PECVD) technique at the frequency 13.56 MHz from 100% SiH<sub>4</sub> at 200 °C. We used fused quartz for substrates. The films prepared were of a thickness of about 5000 Å, possessing parameters typical of standard *a*-Si:H films: the conductivity of the order of  $10^{-10}$  Ω<sup>-1</sup> cm<sup>-1</sup> (at room temperature) and optical gap 1.7-1.72 eV.

The Raman measurements were carried out in the backscattering geometry using computer-controlled DFS-24 double monochromator with a cooled photomultiplier tube and a photon counting system. The spectral resolution was 5 cm<sup>-1</sup> and the scanning accuracy was about 1 cm<sup>-1</sup>. The spectra were excited by the 4888-Å line of an argon-ion laser. Also, laser-induced heating was used to change the local temperature of the sample. The

laser beam was focused in a 30–100-Å spot by means of lenses. Estimated via the ratio of anti-Stokes and Stokes intensities, the temperature varied from 30 to 1200 °C depending on the laser power and the spot diameter. The following measurements were typically conducted. First, the sample was heated by a power laser beam during the scanning time (200 s). After that the laser power was reduced to  $\lesssim 10$  mW (at which power no heating took place) and the measurements were taken again. The latter step implies the crystallization to be an irreversible effect, surviving in spite of a posterior cooling. To check the validity of the laser-induced heating procedure a conventional thermal annealing was performed during the same time 200 s at different temperatures.

Shown in Fig. 2 are Raman spectra measured at various temperatures. Associated with the crystalline phase is the high-frequency peak that appears at the temperatures exceeding 500 °C. Although its relative intensity everywhere increases with the temperature increase, its maximum position shifts with the temperature non-monotonously. Namely, the blueshift at  $T \leq 730$  °C turns into a redshift one at higher temperatures. Both the redshift and concomitant peak broadening result from the increase in anharmonic processes which have nothing to do with crystallites growth. That is why from here on we restrict ourselves to considering the Raman spectra measured after the samples have been cooled from a given temperature  $T$  to room temperature by reducing the laser power. Corresponding to  $T = 730$  °C such a spectrum is shown in Fig. 2 by a dashed line. In what follows each

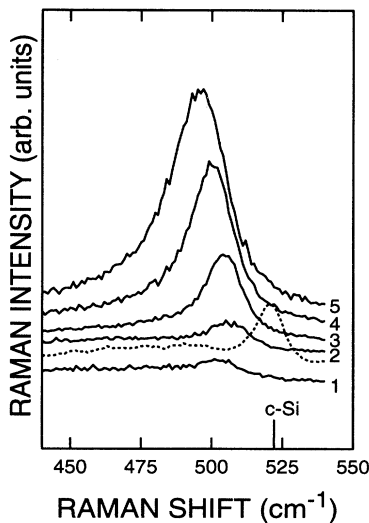


FIG. 2. Raman spectra of  $a$ -Si:H annealed at different temperatures for 200 s. Solid lines correspond to the measurements taken at the annealing temperatures (1) 627 °C, (2) 730 °C, (3) 890 °C, (4) 1030 °C, (5) 1280 °C. A dashed line shows the spectrum (multiplied by a factor 5) measured at room temperature after annealing at 730 °C for 200 s. The phonon frequency corresponding to  $c$ -Si at room temperature is marked.

Raman spectrum is characterized by the maximum temperature  $T$  to which a particular sample has been heated.

More in detail measured at room temperature Raman spectrum is shown in Fig. 3. The results are directly comparable with Eqs. (16), (17), in which the following experimental parameters have been used:  $\omega_0 = 522$   $\text{cm}^{-1}$ ,  $\Gamma_c = 5$   $\text{cm}^{-1}$ ,  $\omega_d = 480$   $\text{cm}^{-1}$ ,  $\Gamma_d = 70$   $\text{cm}^{-1}$ . Also, we used the dispersion  $\omega(q) = \omega_0(1 - 0.18q^2)$  with  $q_{\text{max}} = 0.8$ , where  $q$  is expressed in units  $2\pi/a$ , and  $a = 5.4$  Å is the lattice parameter for bulk the crystalline silicon.<sup>24</sup> The best fit (solid line in Fig. 3) was achieved by putting  $R = 40$  Å which value we consider as the average crystallite radius related to the annealing temperature  $T = 730$  °C and annealing time  $t = 200$  s.

In the same way we estimated the average crystallites radii corresponding to different annealing temperatures  $T$ . The results are given in Fig. 4 for both laser and thermally annealed samples. It is seen from Fig. 4 that the two procedures lead to results which are in satisfactory agreement. It is worth noting that, thermally annealed at  $T \approx 800$  °C, the samples showed a light yellow coloring which is typical of microcrystalline silicon. The data in Fig. 4 correspond to the annealing time  $t = 200$  s.

Figure 5 shows the evolution of Raman spectra with a time at the laser annealing temperature  $T = 730$  °C. As is seen from Fig. 5, related to the crystalline phase, the narrow peak arises at the early stage of annealing. Its intensity increases rather fast initially. However, the increase slows down considerably as time goes on. Plotted in Fig. 6 these data clearly show two different stages, fast and slow, in the peak intensity kinetics. The time dependence is approximately linear in  $t$  at the first stage, while it can be equally described by either slow linear or logarithmic dependence. Further measurements in the long-time range must be called on to verify the logarithmic

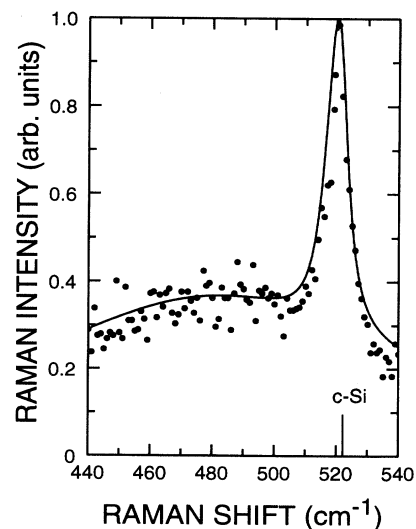


FIG. 3. Raman spectrum measured at room temperature (symbols) in  $a$ -Si:H annealed at 730 °C for 200 s. The solid line is a fit according to Eq. (16) and is discussed in the text.

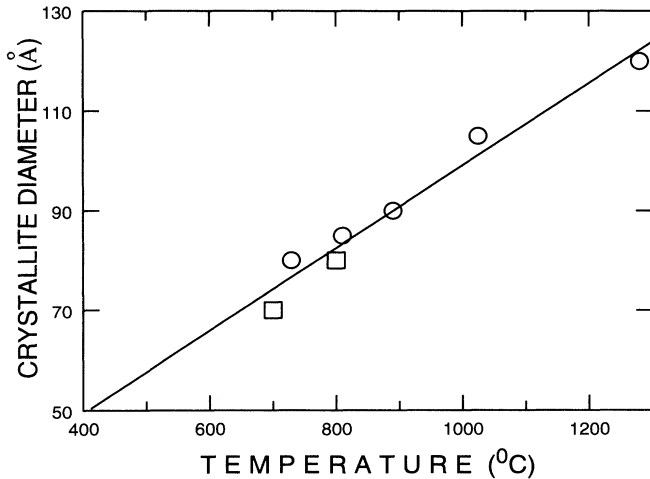


FIG. 4. The average crystallite diameter as a function of temperature.

mic dependence predicted by the theory above.

This result should be noted. As is seen from Fig. 5, the amorphous (broad) component of Raman line remains the same both in its shape and intensity for all the annealing times within the accuracy of our experiments. This result clearly shows that the amorphous phase volume fraction remains almost the same, in spite of the fact that the crystallites cause strong light scattering, resulting in the narrow Raman line component. Hence, the scattering per unit volume of a crystalline phase is much stronger than that of the amorphous phase. The latter conclusion agrees with the prediction of Eq. (18) and the

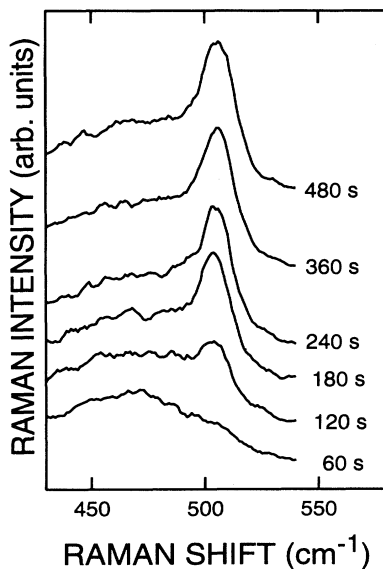


FIG. 5. Raman spectra of *a*-Si:H annealed at 730 °C depending on the annealing time.

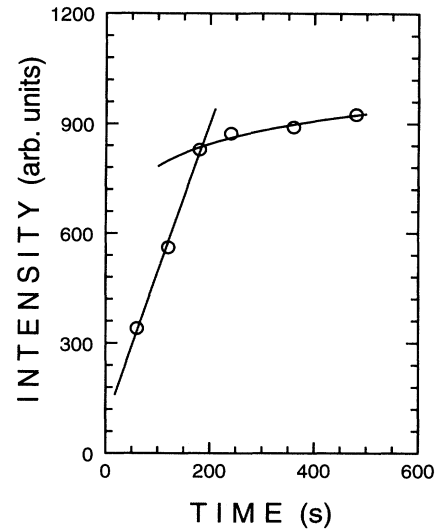


FIG. 6. The integral intensity of crystalline (narrow) component of Raman line as a function of time.

related discussion in Sec. III A.

Along the same experimental lines the measurements of crystallization kinetics were attempted at higher temperatures 1000 and 1200 °C. In both cases the Raman components related to the crystalline phase showed a small increase of the order of 10% within relatively narrow initial time intervals, after which no visible change in the crystalline phase content was detected on a scale of the experimental times  $t \leq 10$  min. In both cases the estimated average crystallites radius was close to 60 Å.

### C. Discussion

The above data enable one to decide between the two scenarios of crystallization described in Sec. II. We note that neither the concentration nor radii of the crystalline embryos are found to be linear in time and exponential in temperature. Also, no evidence of nuclear radii exponentially exceeding their initial values was observed. Therefore, none of the predictions of the standard crystallization scenarios predictions is confirmed experimentally.

It should be stressed that the latter conclusion holds true apart from the way in which the Raman line intensities are analyzed. Both the standard interpretation (implying the intensities to be linear in corresponding volume fractions) and its modification in Sec. III A (based on the quadratic dependences) lead to the same conclusion that the standard approach to crystallization is inconsistent with the above data on amorphous silicon.

On the other hand, there are at least two facts testifying in the favor of the alternative scenario based on accounting for the disorder effects in crystallization. These are (1) the logarithmically weak time dependence of the crystalline volume fraction and (2) the increase in the av-

erage crystallite radius by a factor of 2 during the crystallization process. Although the above data show the presence of relatively fast kinetics at the early stage of crystallization, they are not sufficient to make a definite conclusion about its time dependence. We can only note that as linearly extrapolated to zero time the data lead us to an absurd conclusion that the crystalline volume fraction is negative at  $t = 0$ . The latter means that at short times (beyond the experimental times) the kinetics must be faster than observed. Therefore, the prediction about the nucleation kinetics nonlinear in time is confirmed qualitatively.

Supposing the second scenario of crystallization is valid, one can estimate different material parameters and to test the self-consistency of the approach presented. By linear extrapolating the data in Fig. 4 into the region  $T = 400\text{--}500^\circ\text{C}$  where the crystallization is known to occur<sup>12</sup> one can estimate the critical nuclear radius as  $R_c \approx 27 \pm 3 \text{ \AA}$  [that the dependence  $R(T)$  is slightly nonlinear as predicted by Eq. (13) does not influence the latter estimate, since the interval of extrapolation is relatively narrow; the nonlinearity is taken into account in what follows].

Given the critical radius, an estimate of the correlation radius  $r_c$  can be attempted based on Eq. (18) and the data on  $I_c/I_a$  corresponding to different radii shown in Fig. 4. Both the ratios  $I_c/I_a$  and crystallites radii were extracted from the same Raman spectra. Taking into account that the crystalline volume fraction is close to 0.1 at  $R = R_c$  (see Sec. IID above) Eq. (18) becomes

$$\frac{I_c}{I_a} = \frac{\chi' x^6}{1 - 0.1x^3}, \quad x \equiv \frac{R}{R_c}, \quad \chi' = 0.1\chi \left(\frac{R_c}{r_c}\right)^3. \quad (19)$$

One can extract  $r_c$  by fitting the data on  $I_c/I_a$  with Eq. (19). Shown in Fig. 7 the fit gives  $r_c = 12 \pm 3 \text{ \AA}$ .

To check the time dependence  $R(t)$  given by Eq. (13) the value  $\sqrt{4\pi(R^3 - R_c^3)/3r_c^3}$  versus  $T \ln(u_0 t/a)$  is plot-

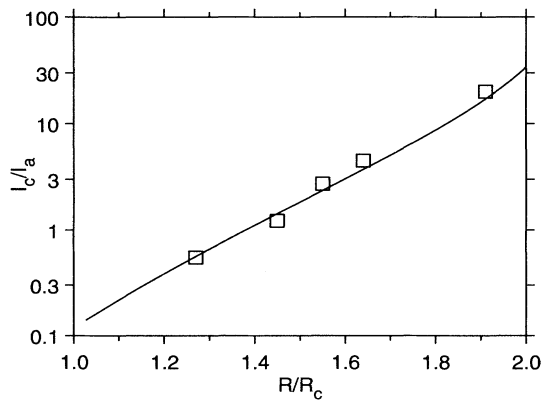


FIG. 7. The ratio of the integral intensities of crystalline ( $I_c$ ) and amorphous ( $I_a$ ) Raman line components as obtained from Eq. (19) with  $r_c = 12 \text{ \AA}$  (solid line) and by means of direct measurements (squares).

ted in Fig. 8 with  $u_0 = 10^5 \text{ cm/s}$  (an uncertainty in  $u_0$  does not affect the results considerably, since it is under the logarithm). It is clearly seen that taken at different temperatures and times the data scale as  $T \ln t$ , in agreement with Eq. (13). As extracted from the slope in Fig. 8 the characteristic dispersion in the diffusion barriers is  $v \approx 0.1 \text{ eV}$ , which value seems reasonable in light of the discussion in Sec. II. Also, the intersection point gives  $V/v \approx 10$ ; i.e., the average diffusion barrier is estimated as  $\approx 1 \text{ eV}$ .

As mentioned in Sec. IIIB for the crystallization kinetics measurements taken at high temperatures, they can be interpreted as corresponding to the ripening stage. Indeed, estimated from Eq. (18) the saturated crystalline volume fraction was about 70%, while the average crystallites radius close to  $60 \text{ \AA}$ , twice as large as  $R_c$ . These values are in a fair agreement with those predicted by our model for the beginning of ripening stage. The apparent saturation in the crystalline volume fraction can be then regarded as a very slow ripening kinetics. This interpretation agrees also with the prediction of Eq. (14) which states that the nucleation time decreases exponentially with temperature. Correspondingly, at high temperatures the nucleation stage could be hardly observed on a time scale of our experiments.

Less reliable are the estimates based on the fast kinetics region data in Fig. 6. Following the model in Sec. II that region corresponds to the nucleation stage of crystallization. Then, substituting  $v_c = 0.1$  in Eq. (11) and noting that  $dv_c/v_c dt = dI_c/2I_c dt$  can be extracted from the data in Fig. 6, one estimates  $E_0 \approx 6kT \approx 0.5 \text{ eV}$ .

Given the energies  $V$  and  $E_0$ , we can estimate the nucleation barrier  $W$  by substituting the nucleation time  $\Delta t_1$  in Eq. (14), which gives  $W \approx 5 \text{ eV}$ . Taking into account that  $W = 4\pi R_c^2 \sigma/3$  we find also  $\sigma a^2 \approx 0.05 \text{ eV}$ . From that we get  $\mu a^3 = 2\sigma a^3/R_c \approx 2 \times 10^{-2} \text{ eV}$ . The values of the parameters estimated above are summarized in Table I. Thus, all the model parameters characteriz-

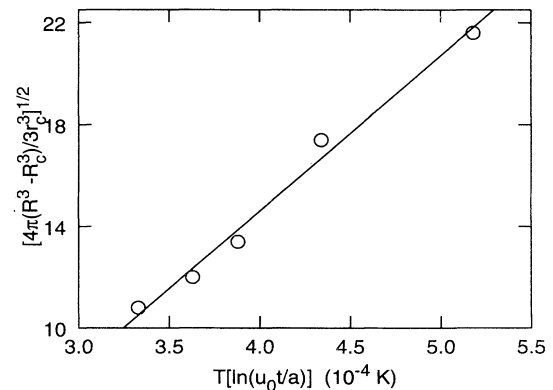


FIG. 8. Scaling of the crystallites averaged radii measured at different temperatures and annealing times as discussed in the text.

TABLE I. Parameters of  $a$ -Si:H as estimated from the fit of the model proposed with experimental data: critical nucleation radius  $R_c$ , correlation radius of the disorder  $r_c$ , barrier to nucleation  $W$ , surface energy per elemental cell  $\sigma a^2$ , energy gain due to crystallization per elemental cell  $\mu a^3$ , average diffusion barrier  $V$ , and dispersion in atomic energies  $v$ .

$R_c$ (Å)	$r_c$ (Å)	$W$ (eV)	$\sigma a^2$ (eV)	$\mu a^3$ (eV)	$V$ (eV)	$v$ (eV)
$27 \pm 3$	$12 \pm 3$	$5 \pm 0.7$	$(5 \pm 1) \times 10^{-2}$	$(2 \pm 0.5) \times 10^{-2}$	$1.0 \pm 0.3$	$0.1 \pm 0.02$

ing crystallization in  $a$ -Si:H are estimated experimentally. These estimates do not contradict to those obtained in Sec. IIB by means of simple physical arguments.

It should be noted that the above interpretation implies the crystallization to be a polymorphic one: without any change in chemical composition. That such a crystallization is the case for  $a$ -Si:H is not immediately apparent, since hydrogen diffusion cannot be ruled out *a posteriori*. However, there is considerable evidence<sup>12,33</sup> for hydrogen effusion from  $a$ -Si:H at  $T \gtrsim 600$  °C. Since the annealing temperatures used in our experiments were considerably higher than 600 °C, we believe that our data bear on the polymorphic crystallization.

#### IV. CONCLUSIONS

We have presented a model of crystallization in disordered solids which predicts the crystallization kinetics that differs dramatically from the standard approach predictions. Even a relatively small disorder is shown to affect crystallization considerably. The model reveals clearly divided nucleation, growth, and ripening stages in crystallization processes and establishes the parameters governing the kinetics at all of the stages. It accounts for the limited small volume fraction available for nucleation at the first stage. Also, it accounts for the logarithmic time dependences of crystallite radii observed at the growth stage and the temperature scaling of their magnitudes.

The results of Raman–light-scattering experiments designed to test various predictions of the model are pre-

sented for  $a$ -Si:H subjected to crystallization. We have shown that the standard predictions lack support from the data, while they all can be explained in the framework of our model. When these results are compared with the model, it is possible to estimate the numerical values of parameters governing the crystallization in  $a$ -Si:H. A set of parameters has been estimated in this way including both the crystallization parameters and the characteristics of the disorder: correlation radius and fluctuations in atomic energies.

Taken together with the results of recent theoretical considerations in Refs. 4 and 5 the investigation presented shows that the first-order phase transition kinetics in disordered solids differs qualitatively from the classic theories predictions. Such a kinetics is perhaps one of the most prominent examples of the disorder-induced effects in solids. Generally, it has much in common with the electron kinetics in disordered solids. In both cases the disorder brings into existence and/or changes significantly some potential barriers governing the kinetics; also, in both cases the disorder makes the processes localized as compared to those of homogeneous media.

#### ACKNOWLEDGMENTS

This work was supported by the Russian R&D Program “Fullerenes and Atomic Clusters” under Grant No. 29. We are grateful to M. Grimsditch for stimulating discussions. One of us (V.G.K.) also acknowledges a travel grant (No. 931647) from the North Atlantic Treaty Organization.

<sup>1</sup> H. Rawson, *Glass-Forming Systems* (Academic Press, London, 1967).

<sup>2</sup> M. E. Fine, *Phase Transformation in Condensed Systems* (MacMillan, New York, 1964).

<sup>3</sup> U. Koster and U. Herold, in *Glassy Metals 1*, edited by H.-J. Guntherodt and H. Beck (Springer-Verlag, Berlin, 1981).

<sup>4</sup> V. G. Karpov, Phys. Rev. B **50**, 9124 (1994).

<sup>5</sup> V. G. Karpov (unpublished).

<sup>6</sup> By assuming that the short-range topology in an amorphous solid is the same as in the corresponding crystal we imply the materials like  $a$ -SiO<sub>2</sub>,  $a$ -Si, etc., as opposed to metallic glasses where the short-range order may differ considerably from that of related crystals.

<sup>7</sup> In some multicomponent systems the nuclear growth is de-

termined by the diffusion process (Ref. 3), which leads to  $R(t) \propto \sqrt{t}$ .

<sup>8</sup> A general case  $E \leq W$  has been treated in Ref. 4.

<sup>9</sup> S. R. Elliott, Europhys. Lett. **19**, 201 (1992).

<sup>10</sup> D. L. Price, S. Moss, R. Reijers, M.-L. Saboungi, and S. Susman, J. Phys. Condens. Matter **1**, 1005 (1989).

<sup>11</sup> L. Börjesson, A. K. Hassan, J. Swenson, L. M. Torell, and A. Fontana, Phys. Rev. Lett. **70**, 1275 (1993).

<sup>12</sup> *The Physics of Hydrogenated Amorphous Silicon*, edited by J. D. Joannopoulos and G. Lucovsky (Springer, New York, 1984).

<sup>13</sup> H. R. Schober and B. B. Liard, Phys. Rev. B **44**, 6746 (1991).

<sup>14</sup> G. A. Dyadyna, V. G. Karpov, V. N. Solov'ev, and V. A. Khrisanov, Fiz. Tverd. Tela (Leningrad) **31**, 148 (1989)

- [Sov. Phys. Solid State, **31**, 629 (1989)].
- <sup>15</sup> V. G. Karpov and M. Grimsditch, Phys. Rev. B **48**, 6941 (1993).
- <sup>16</sup> Rayleigh, Lord, Philos. Mag. **41**, 274 (1871); **41**, 447 (1871); G. Mie, Ann. Phys. (Leipzig) **25**, 377 (1908).
- <sup>17</sup> M. Born and E. Wolf, *Principles of Optics* (Pergamon, London, 1968).
- <sup>18</sup> L. D. Landau and E. M. Lifshitz, *Electrodynamics of Continuous Media* (Pergamon, London, 1986).
- <sup>19</sup> M. Cardona, in *Light Scattering in Solids II*, edited by M. Cardona and G. Guetherodt (Springer, New York, 1982).
- <sup>20</sup> Z. Iqbal, S. Veprek, A. P. Webb, and P. Capezzuto, Solid State Commun. **37**, 993 (1981).
- <sup>21</sup> M. H. Brodsky, in *Light Scattering in Solids II*, edited by M. Cardona and G. Guetherodt (Springer, New York, 1982).
- <sup>22</sup> H. Richter, Z. P. Wang, and L. Ley, Solid State Commun. **39**, 625 (1981).
- <sup>23</sup> I. H. Campbell and P. M. Fauchet, Solid State Commun. **58**, 739 (1986).
- <sup>24</sup> A. Roy, K. Jayaram, and A. K. Sood, Solid State Commun. **89**, 229 (1994).
- <sup>25</sup> S. M. Prokes and O. J. Glembocki, Phys. Rev. B **49**, 2238 (1994).
- <sup>26</sup> Y. Kanemitsu, H. Uto, Y. Masumoto, T. Matsumoto, T. Futagi, and H. Mimura, Phys. Rev. B **48**, 2827 (1993).
- <sup>27</sup> S. Veprek, F. A. Sarott, and Z. Iqbal, Phys. Rev. B **36**, 3344 (1987).
- <sup>28</sup> E. Bustarret, M. Ligeon, J. C. Bruyere, F. Muller, R. Herino, F. Gaspard, L. Ortega, and M. Stutzmann, Appl. Phys. Lett. **61**, 1552 (1992).
- <sup>29</sup> Y. He, C. Yin, G. Cheng, L. Wang, X. Liu, and G. Y. Hu, J. Appl. Phys. **75**, 797 (1994).
- <sup>30</sup> R. Tsu, J. Gonzalez-Fernandez, S. S. Chao, S. C. Lee, and K. Tanaka, Appl. Phys. Lett. **40**, 534 (1982).
- <sup>31</sup> D. Beeman, R. Tsu, and M. F. Tporpe, Phys. Rev. B **32**, 874 (1985).
- <sup>32</sup> E. Bustarret, M. Hichicha, and M. Burnell, Appl. Phys. Lett. **52**, 1675 (1988).
- <sup>33</sup> W. Beyer, in *Tetrahedrally-Bonded Amorphous Semiconductors*, edited by D. Adler and H. Fritzsche (Plenum Press, New York, 1985).